Mechanism of Anode Break Stimulation in the Heart

Ravi Ranjan,* Nipavan Chiamvimonvat,# Nitish V. Thakor,* Gordon F. Tomaselli,§ Eduardo Marban§
*Department of Biomedical Engineering, Johns Hopkins University School of Medicine, Baltimore, Maryland 21205; #Division of Cardiology University of Cincinnati, Cincinnati, Ohio 45267; and §Section of Molecular and Cellular Cardiology, Department of Medicine, Johns Hopkins University School of Medicine, Baltimore, Maryland 21205 USA

ABSTRACT Anodal stimulation is routinely observed in cardiac tissue, but only recently has a mechanism been proposed. The bidomain cardiac tissue model proposes that virtual cathodes induced at sites distant from the electrode initiate the depolarization. In contrast, none of the existing cardiac action potential models (Luo-Rudy phase I and II, or Oxsoft) predict anodal stimulation at the single-cell level. To determine whether anodal stimulation has a cellular basis, we measured membrane potential and membrane current in mammalian ventricular myocytes by using whole-cell patch clamp. Anode break responses can be readily elicited in single ventricular cells. The basis of this anodal stimulation in single cells is recruitment of the hyperpolarization-activated inward current I_f. The threshold of activation for I_f is −80 mV in rat cells and −120 mV in guinea pig or canine cells. Persistent I_f "tail" current upon release of the hyperpolarization drives the transmembrane potential toward the threshold of sodium channels, initiating an action potential. Time-dependent block of the inward rectifier, I_{K1}, at hyperpolarized potentials decreases membrane conductance and thereby potentiates the ability of I_f to depolarize the cell on the break of an anodal pulse. Inclusion of I_f, as well as the block and unblock kinetics of I_{K1}, in the existing Luo-Rudy action potential model faithfully reproduces anode break stimulation. Thus active cellular properties suffice to explain anode break stimulation in cardiac tissue.

INTRODUCTION

The heart can be stimulated by either cathodal or anodal stimulation (Cranefield et al., 1957; Dekker, 1970). Cathodal stimulation of the heart or any other excitable tissue is readily explained by direct depolarization of the cells in the region under the electrode (Hoffman and Cranefield, 1960). Anodal stimulation results in hyperpolarization of the underlying tissue (Brooks et al., 1955; Cranefield et al., 1957), so that the ability to trigger an action potential is paradoxical. Anodal stimulation can occur during the stimulus pulse (make stimulation) or upon the termination of the pulse (break stimulation) (Dekker, 1970). Recently, anodal stimulation of cardiac tissue has been explained using bidomain models of cardiac tissue (Pollard et al., 1992; Henriquez, 1993). Bidomain models postulate different electrical anisotropies in the intracellular and interstitial domains of the heart (Plonsey and Barr, 1984; Roth, 1988; Henriquez et al., 1990). The unequal anisotropy in the two domains leads to marked inhomogeneities in the induced membrane potential around the stimulating electrode (Roth and Wikswo, 1994; Sepulveda and Wikswo, 1994). During anodal stimulation, a "dog bone"-shaped region of the tissue underlying the stimulating electrode becomes hyperpolarized, whereas regions lying in the convexity of the dog bone become depolarized and are referred to as "virtual cathodes" (Sepulveda et al., 1989; Roth, 1992). It is proposed that, during anodal stimulation, the excitation wavefront starts from these virtual cathodes (Roth, 1994, 1996; Wikswo, 1994). Anodal stimulation during the stimulating pulse (anode make stimulation) can be explained by this model. For anode break stimulation, the bidomain model assumes that a steady state has been reached during the anodal pulse with regions of hyperpolarized and depolarized tissue; upon termination of the stimulus pulse, excitation propagates from the hyperpolarized tissue region as a result of depolarization extending from the virtual cathodes (Roth, 1995; Wikswo et al., 1995).

Recently a hyperpolarization-activated current was identified in normal (Yu et al., 1995; Cerbai et al., 1996) and failing (Cerbai et al., 1994, 1997) ventricular myocytes. Except for its voltage dependence, this current appears to be identical to the I_f described in Purkinje fibers and in nodal cells, but it has not yet been included in ventricular action potential models. Another current whose properties change with hyperpolarization is the inward rectifier, I_{K1}. At hyperpolarized potentials the current carried by I_{K1} channels is blocked in a time-dependent manner (Carmeliet, 1980; Biermans et al., 1987; Mitra and Morad, 1991). If the unblocking of this channel at depolarized potentials is time-dependent as well, it could play a significant role in bringing about anodal stimulation. We therefore investigated the active membrane properties recruited during and after hyperpolarization as a mechanism for anodal stimulation. Appropriate modifications were made in the Luo-Rudy phase 1 action potential model (Luo and Rudy, 1991) to better reflect these ionic currents. A preliminary report has appeared (Ranjan et al., 1997).

Received for publication 10 October 1997 and in final form 15 December 1997.

Address reprint requests to Dr. Eduardo Marban, Section of Molecular and Cellular Cardiology, 844 Ross Bldg., Johns Hopkins University School of Medicine, 720 Rutland Ave., Baltimore, MD 21205. Tel.: 410-955-2776; Fax: 410-955-7953; E-mail: marban@welchlink.welch.jhu.edu.

0006-3495/98/04/1850/14 $2.00

MATERIALS AND METHODS

Isolation of ventricular myocytes

Canine, guinea pig, and rat ventricular myocytes were used for the study. Adult mongrel dogs weighing 20–30 kg and Wistar-Kyoto (WKY) and Fisher-344 (F344) rats ranging in age from 6 to 22 months were used. Canine ventricular myocytes were isolated as previously described (Kääb et al., 1996). Briefly, the dogs were sedated with sodium thiamylol and anesthetized with 1–2% halothane. The chest cavity was opened by performing a left lateral thoracotomy and flooded with ice-cold saline. After banding the great vessels, the coronary arteries were perfused retrogradely, with cold cardioplegic solution containing (in mM) 110 NaCl, 16 KCl, 16 $MgCl_2$, 10 $NaHCO_3$, and 1 $CaCl_2$, with a pH of 7.4. After diastolic cardiac arrest, the heart was quickly excised and submerged in cold cardioplegic solution. The area of the myocardium perfused by the left anterior descending coronary artery (LAD) from the aortic root to the apex was excised and then perfused via the LAD at a rate of 15 ml/min with a Ca^{2+}-free solution containing (in mM) 138 NaCl, 4 KCl, 1 $MgCl_2$, 10 glucose, 0.33 NaH_2PO_4, and 10 HEPES, with a pH of 7.3. After 30 min of perfusion, the myocardial segment was perfused for another 40 min with the same solution containing collagenase (type I, 178 units/ml; Worthington Biochemical Corp) and protease (type XIV, 0.12 mg/ml; Sigma Chemical Co). The myocardium was then washed for 15 min with Tyrode's solution containing 200 μM Ca^{2+}. All solutions were oxygenated with 100% O_2 and kept at 37°C. After perfusion, cells were mechanically desegregated from chunks of well-digested myocardial tissue from the middle of the ventricular wall, filtered through a nylon mesh, and stored at room temperature in Tyrode's solution containing 2.0 mM Ca^{2+} until use.

Rat and guinea pig ventricular myocytes were isolated by conventional enzymatic dissociation techniques (Liu et al., 1996). Briefly, the heart was excised via a median sternotomy from animals anesthetized with pentobarbital (60 mg/kg i.p.). The heart was then perfused at 37°C with modified Krebs solution composed of (in mM) 120 NaCl, 5 KCl, 1.2 $MgCl_2$, 1.2 Na_2SO_4, 2 NaH_2PO_4, 20 $NaHPO_3$, 0.5 $CaCl_2$, and 10 glucose bubbled with 95% O_2/5% CO_2. After 5 min, the heart was perfused without Ca^{2+} for another 5 min and then switched to a Krebs containing collagenase (1 mg/ml; Boehringer Mannheim, Germany) and protease (0.1 mg/ml; Sigma Chemical Co.). Perfusion with the collagenase solution was carried out for another 10–15 min at a perfusion pressure of ~80 mm Hg, after which the heart was removed from the perfusion apparatus, the atria removed, and the ventricles minced and incubated in the collagenase-containing solution for another 10–15 min. Cells were then filtered through a mesh and stored in a solution containing (in mM) 140 NaCl, 5 KCl, 1 $MgCl_2$, 10 HEPES, 10 glucose, and 1.5 $CaCl_2$ at room temperature. Only Ca^{2+}-tolerant cells with uniform sarcomeric appearance and nonrounded edges were chosen for the study. The cells were used within 24 h of isolation.

Electrophysiological studies

Isolated myocytes were placed in a bath mounted on the stage of an inverted microscope. To study the response to anodal stimulation, transmembrane potential was recorded under current clamp conditions in the whole-cell configuration of the patch-clamp technique (Hamill et al., 1981) in normal physiological Tyrode's solution of the following composition (in mM): 140 NaCl, 5 KCl, 1 $MgCl_2$, 10 HEPES, 10 glucose, and 1.8 $CaCl_2$ (pH 7.4 with NaOH). The pipettes, made of borosilicate glass, had resistances of 2–4 MΩ when filled with the standard internal solution containing (mM): 6 NaCl, 130 K-aspartate, 2 $MgCl_2$, 5 $CaCl_2$, 11 EGTA, 2 Mg-ATP, 0.2 Na-cAMP, and 10 HEPES (pH 7.2 with KOH). Patch-clamp amplifiers Axopatch 200A and Axoclamp 2A (Axon Instruments) were used to make the recordings with the filter cutoff set at 2 kHz. All of the recordings were made at room temperature (21–22°C).

Membrane currents were recorded using the whole-cell configuration of the patch-clamp technique. After we gained intracellular access, cell capacitance was calculated by integrating the area under the uncompensated capacity transient elicited by a 10-mV step from a holding potential of −80 mV.

The largest current at hyperpolarized potentials is I_{K1}. This current was studied under the same ionic conditions as action potentials, at different hyperpolarizing potentials to quantify the time and voltage dependence of block. To study the time-dependent unblocking of this current, cells were studied under the ionic conditions described above, with 100 μM tetrodotoxin (Sigma Chemical Co.) added to the bath solution to reduce the sodium current at potentials near its threshold. During quantification of I_{K1} block and unblock kinetics, potential interference from I_f was minimized by using pulse protocols that were too brief or insufficiently negative to elicit I_f.

The modified bath solution used to study I_f had the following composition (in mM): 140 NaCl, 5 KCl, 1 $MgCl_2$, 10 HEPES, 10 glucose, 1.8 $CaCl_2$, 2 $MnCl_2$, 0.1 $CdCl_2$, 8 $BaCl_2$ (pH 7.4 with NaOH). Ba^{2+} was used to block I_{K1} and Mn^{2+} and Cd^{2+} to reduce Ca^{2+} currents, which could overlap with and obscure the tail currents. This ionic composition has been used in earlier studies of I_f (Yu et al., 1993, 1995; Cerbai et al., 1994). The voltage dependence of activation was determined from the tail current amplitude after holding the cell at different hyperpolarizing potentials to activate the current. The ionic selectivity of I_f was determined by changing the external ionic concentrations of sodium and potassium, and determining the reversal potential of the instantaneous tail current after activating the current by holding the cell at hyperpolarized potentials. *N*-Methyl glucamine (NMG) was used to replace external sodium to maintain the osmolarity of the solution.

Action potential model

The action potential model developed by Luo and Rudy (1991) was implemented and modified. The ionic currents in the model include a fast sodium current, a slow inward current, a time-dependent potassium current, a plateau potassium current, a time-independent background current, and a time-independent inwardly rectifying potassium current to represent I_{K1}. The time-independent I_{K1} was modified to include the hyperpolarization-induced time-dependent blocking and the subsequent unblocking of the channel at depolarized potentials. The modification was based on a Hodgkin-Huxley-type gating formalism in which a gating variable (y) is governed by a differential equation of the form

$$\frac{dy}{dt} = \frac{(y_\infty - y)}{\tau_y}$$

where τ_y is the time constant and y_∞ is the steady-state value of y.

The gating variable added for the inward rectifier current ($K1$) was experimentally determined to be governed by the equations given below. $K1_\infty$ was determined by fitting a curve to the normalized steady-state conductance curve for I_{K1}. τ_{K1_∞} was determined by fitting a curve to the time constants determined for different test potentials:

$$K1_\infty = 1 + \frac{-0.9075}{1 + \exp\left(\frac{V + 117.1}{10.37}\right)}$$

For $V \le E_K$,

$$\tau_{K1_\infty} = 7.0602 \exp\left(\frac{V + 200.0}{26.22}\right) \text{ ms}$$

where V is the transmembrane potential (in mV) and E_K is the reversal for potassium ions. Because the hyperpolarization-induced blocking is presumably mediated by external cations present in the solution (Carmeliet, 1980; Biermans et al., 1989), the time constant of blocking/unblocking was made symmetrical about the reversal of potassium ions.

I_f was also included in the model, based on the "funny current" formalism in the Purkinje fiber model developed by DiFrancesco and Noble (1985). The time constant of I_f gating determined experimentally at room temperature was adjusted for use in the model at 37°C by applying a Q_{10} of 3.0, based on published results (Hart, 1983).

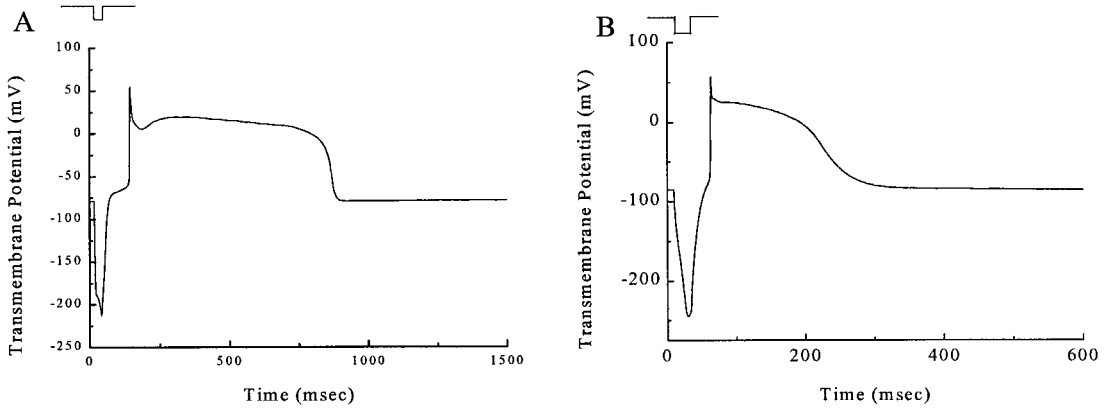

FIGURE 1 Action potentials induced by anodal stimulation in (*A*) canine and (*B*) rat ventricular myocytes. The time for which the stimulus was applied to the cells is indicated by the bar on top of the figures. A 50-ms pulse was applied to the canine cell and a 20-ms pulse to the rat cell.

The gating variable (f) for I_f, per the experimental results, was determined to be governed by the following equations:

$$\alpha_f = 0.01824 \exp\left(-\frac{V + 170.0}{12.36}\right) \text{ms}^{-1}$$

$$\beta_f = \frac{-0.074655}{1 + \exp\left(\frac{V - 29.056}{27.7}\right)} + 0.075955 \text{ ms}^{-1}$$

where

$$\tau_f = \frac{1}{\alpha + \beta}$$

and

$$f_\infty = \frac{\alpha}{\alpha + \beta}.$$

I_f is given by

$$I_f = f(V - E_f)0.1$$

where E_f is the reversal potential for I_f (−29 mV).

The integration algorithm used to solve the system of differential equations was based on a backward Euler method (Press et al., 1992), and the simulations were run on an INDIGO R10000 workstation (Silicon Graphics).

RESULTS

Anode break stimulation in single isolated cells

Current clamp experiments were performed on isolated mammalian cardiac myocytes to test the hypothesis that active membrane properties are involved in anodal excitation. Action potentials were routinely recorded upon the break of anodal stimulation. Fig. 1 shows representative action potentials induced in canine (Fig. 1 *A*) and rat (Fig. 1 *B*) ventricular cells under current clamp conditions with anodal stimulation. During the current injection itself, the membrane simply hyperpolarizes, but after termination of the stimulus the membrane potential reaches threshold and an action potential ensues. The anodally induced action potentials in Fig. 1 are representative of 13 canine and 14 rat cells. Anode break responses were also observed in nine guinea pig ventricular myocytes (data not shown). Thus anode break excitation exists in single isolated ventricular cells from a variety of mammalian species, demonstrating that such excitation need not depend upon passive tissue properties.

Membrane currents during hyperpolarization

To understand the ionic basis of anodal stimulation, we measured membrane currents in isolated mammalian ventricular cells at increasingly negative potentials. I_{K1} is the predominant current at hyperpolarized potentials. Fig. 2 shows the membrane currents activated by hyperpolarization, beginning with a transient spike of capacity current. Thereafter, at −160 mV, I_{K1} turns on and is subsequently blocked in a time-dependent manner. At a more hyperpo-

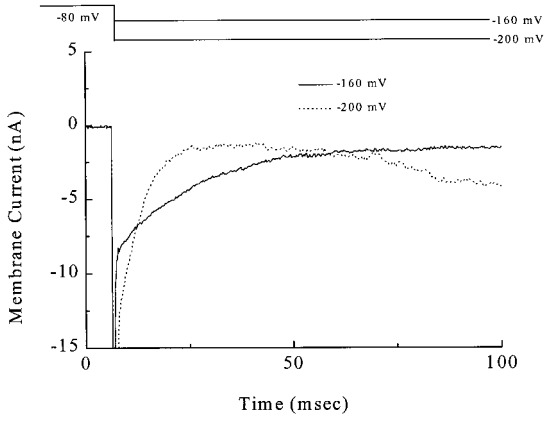

FIGURE 2 Total ionic current in response to hyperpolarizing voltage clamp steps in a canine myocyte under normal physiological ionic conditions. At −160 mV there is a time-dependent blocking of the current carried by the I_{K1} channels. At −200 mV the blocking of I_{K1} is faster, and an inward current (I_f) is activated.

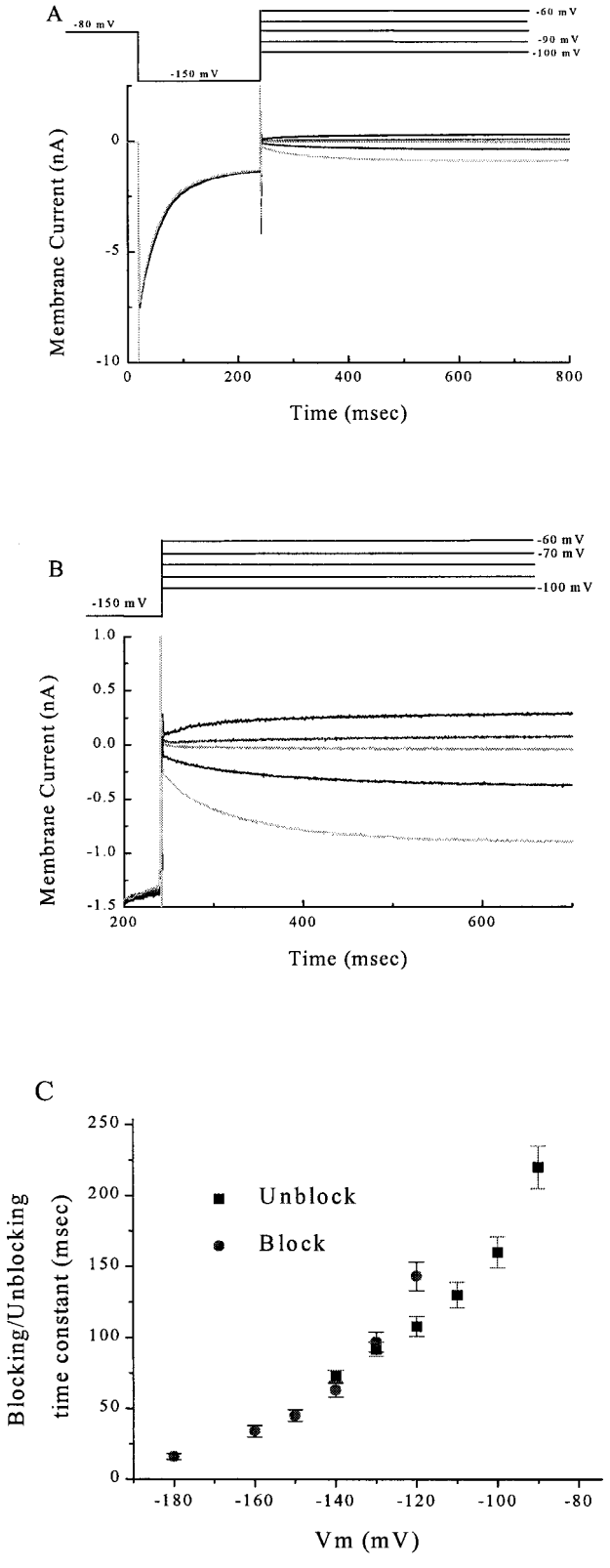

FIGURE 3 Time-dependent unblocking of I_{K1}. (*A*) Current recorded from a rat myocyte held at a hyperpolarizing voltage to induce block and then stepped to a more depolarized tail potential to demonstrate time-dependent unblock of I_{K1}. (*B*) Same as *A*, with an expanded scale to illustrate the unblocking. There is an increase in current with time, and the direction of the current is dependent on whether the pulse is positive or negative to E_K. (*C*) Time constant of I_{K1} block/unblock ($n = 5$). The time constant of block was derived from single exponential fits to the decreasing current profiles at different potentials. Time constant of unblock was derived from single exponential fits to the increasing current profiles at different tail potentials.

larized potential (−200 mV), the decay of I_{K1} is much faster, and there is activation of another inward current, the hyperpolarization-activated current, I_f. Whereas the records shown here are from a dog cell, similar currents were observed in rat and in guinea pig myocytes, albeit with somewhat different voltage dependences for I_f, as discussed below.

To dissect the two current components that change with hyperpolarization, different ionic conditions and voltage clamp protocols were used. I_{K1} was studied at hyperpolarized potentials under physiological ionic conditions. Because the activation and blocking of I_{K1} current are much faster than the reported activation time constant of I_f (DiFrancesco et al., 1986; Yu et al., 1995), all of the I_{K1}-related recordings were made before there was any significant activation of I_f. To isolate I_f, barium was used to block I_{K1}.

Kinetics of I_{K1} block and unblock

To quantify the block of I_{K1} at negative potentials and its subsequent unblock at voltages near the resting potential, voltage clamp experiments were performed. As reported earlier, the block was found to be time- and voltage-dependent, becoming faster and more pronounced as the potential became more negative (Biermans et al., 1989). If the unblocking is time-dependent as well, then the magnitude of I_{K1} will be reduced just after the potential is stepped back to more depolarized levels. This reduction in I_{K1} after the termination of the pulse will facilitate depolarization beyond the resting potential. To test if the unblocking of I_{K1} is indeed time-dependent, the cell was held at −80 mV, stepped to −150 mV until steady-state block was reached, and then stepped back to more depolarized potentials. Fig. 3 *A* shows that, after we stepped back to less negative voltages, there was a time-dependent increase in current as the channels unblocked. The growing current (shown on an expanded scale in Fig. 3 *B*) is inward or outward, depending on whether the pulse is positive or negative with respect to the equilibrium potential for potassium ions (E_K). Both the block and the unblock of the current could be well-fit with single exponentials. The time constants at various potentials for block (*circles*) and unblock (*squares*) are plotted in Fig. 3 *C*.

Characterization of I_f during and after hyperpolarizing steps

We next characterized the hyperpolarization-activated inward current tentatively identified as I_f. Fig. 4 shows the membrane current elicited by hyperpolarization in canine

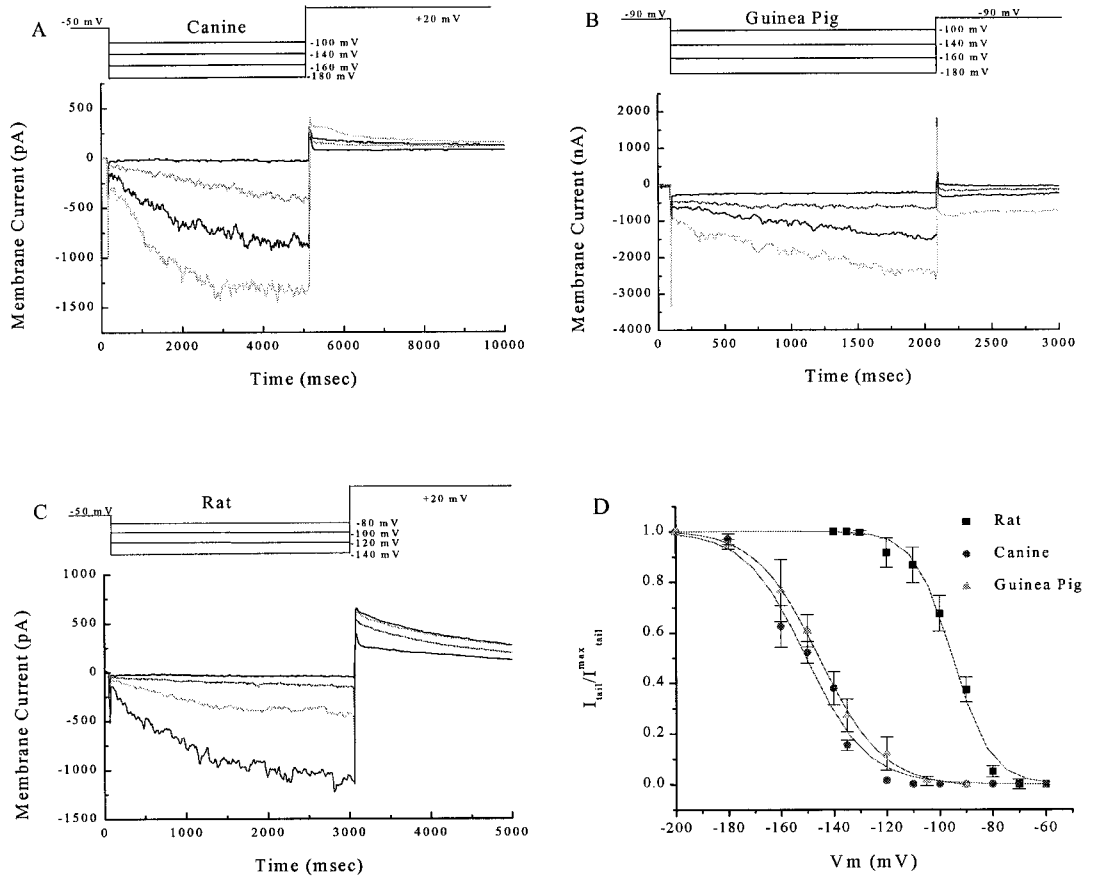

FIGURE 4 I_f in ventricular myocytes. The recordings were made in the presence of 8 mM Ba^{2+} in the bath solution to block I_{K1}. (*A–C*) Representative currents in canine (*A*), guinea pig (*B*), and rat (*C*) ventricular myocyte. (*D*) The activation curve for canine, guinea pig, and rat cells determined from the tail current after different hyperpolarizing pulses activating the current. Data points represent mean ± SD ($n = 5$, $n = 4$ for guinea pig cells). Solid lines represent a sigmoidal fit to the data using the Boltzman equation. $V_{1/2} = -150$ mV for canine cells, −145 mV for guinea pig cells, and −93.9 mV for rats cells with a slope factor of 12.2 mV for canine, 12.0 for guinea pig, and 7.4 mV for rat cells.

(Fig. 4 *A*), guinea pig (Fig. 4 *B*), and rat (Fig. 4 *C*) ventricular myocytes under the ionic conditions identified in Methods (including 8 mM Ba^{2+} to block I_{K1}). A slowly activating inward current is observed. The time constant of activation is similar to that of I_f (DiFrancesco et al., 1986; Yu et al., 1995). Fig. 4 also shows the slowly decaying tail currents in representative canine (Fig. 4 *A*), guinea pig (Fig. 4 *B*), and rat (Fig. 4 *C*) ventricular myocytes. The voltage dependence of activation of the channel (Fig. 4 *D*) was determined by measuring instantaneous tail currents. The time constant of activation was found to be longer in canine and guinea pig than in rat cells, in agreement with published results for I_f (Yu et al., 1995; Cerbai et al., 1996). As is evident from Fig. 4 *D*, the current is activated at more negative potentials in canine and guinea pig than in rat cells. Even though the current is activated at potentials below normal physiological potentials (particularly in canine and guinea pig cells), these potentials are well within the range that is predicted to be achieved in tissue beneath a stimulating electrode (Roth, 1995).

I_f is known to be a relatively nonselective cation channel. The ionic selectivity of the hyperpolarization-activated channel was tested by altering the ionic concentrations in the external solution and then measuring the reversal potential of the instantaneous tail currents. The reversal potential was found to vary in response to changes in the concentrations of external sodium and potassium ions. Table 1 summarizes the reversal potentials measured in solutions of varying ionic concentrations in rat myocytes; these findings are typical of I_f (DiFrancesco, 1981; Yu et al., 1995).

For anodal stimulation, it would be more relevant to the anodal pacing literature (e.g., Furman et al., 1989) to ex-

TABLE 1 Table showing the reversal potential (E_{rev}) of I_f for different external ionic concentrations ($n = 3$)

$[K^+]_0$ (mM)	$[Na^+]_0$ (mM)	E_{rev} (mV)	E_{Na} (mV)	E_K (mV)
25	140	−10	80	−42
5	140	−29	80	−84
5	70	−35	63	−84
5	10	−52	13	−84

E_{Na} (and E_K) is the calculated reversal potential of sodium (and potassium) for the ionic concentration used for that experiment.

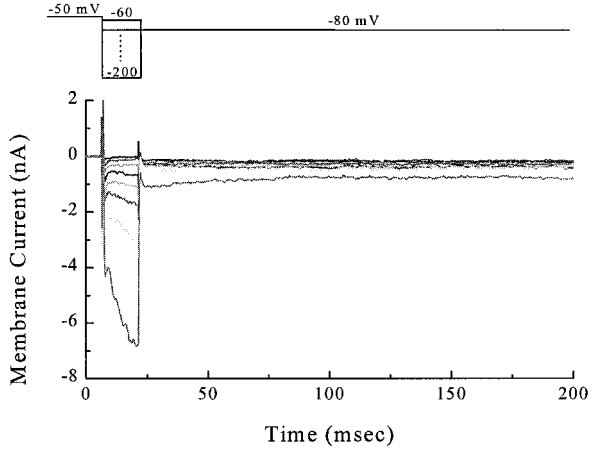

FIGURE 5 Inward current activated by short hyperpolarizing pulses in a rat ventricular myocyte. Short hyperpolarizing pulses of 15 ms were delivered before switching to a test potential of −80 mV. At hyperpolarized potentials an inward current is recorded. The current is larger and the activation more rapid at more negative potentials.

amine the currents activated as a result of short hyperpolarizing pulses. If the current activated during the hyperpolarizing pulse results in persistent inward tail current, it can provide the inward current needed to depolarize the cell to the threshold of sodium current activation. To test whether any inward tail current is activated as a result of hyperpolarizing pulses of short duration, current was recorded in cells held at varying hyperpolarizing potentials for 15 ms and then stepped to a test potential of −80 mV. Fig. 5 shows representative currents recorded from a rat myocyte. At the more hyperpolarized potentials, an inward current activates during the pulse, with corresponding inward tail currents when the cell is stepped back to −80 mV. The deactivation time constant of the current at −80 mV is large, similar to that of I_f (DiFrancesco et al., 1986; Yu et al., 1995).

The presence of I_f is critical at potentials ranging from the resting potential to the threshold for sodium current, as it may provide the inward current needed to depolarize the membrane and trigger an action potential. Thus, we quantified I_f at these potentials. Fig. 6 *A* shows the tail current amplitudes measured at −70 and −90 mV in dog, guinea pig, and rat myocytes after holding the cells at −150 mV for 2 s. Not surprisingly, the tail current is larger in rat than in canine or guinea pig cells: the time constant of activation is longer for dog and guinea pig, and I_f is more fully activated at this potential in rat cells. Nevertheless, Fig. 6 *B* shows that much larger I_f is activated after holding the dog and guinea pig cells for 2 s at −180 mV. The modeling results below confirm that these current densities suffice to initiate anode break excitation.

Strength-duration curve

Because the activation time constant for I_f is on the order of hundreds of milliseconds to seconds at weakly hyperpolarized potentials, longer hyperpolarizing pulses would be expected to result in increased activation of the current. Longer pulses would thus be expected to leave behind larger inward currents after termination of the hyperpolarizing stimuli, hence lowering the threshold for anodal excitation. This prediction was experimentally verified. Fig. 7 shows anodally induced action potentials at threshold using various stimulus durations and strengths (Fig. 7 *A*) and the strength-duration curve (Fig. 7 *B*). Because the activation threshold is more negative and the time constant of activation is longer for canine than for rat cells, a higher stimulus strength would be predicted to be required to excite a dog myocyte. Fig. 7 *B* shows that, for stimuli of the same duration, stronger current pulses are indeed required to excite canine as compared to rat myocytes.

Correlation of I_f magnitude with a measure of stimulation energy

If the presence of I_f is indeed critical in driving the membrane potential to the activation threshold for an action potential, then a larger I_f would be expected to facilitate the depolarization process. For activation of I_f, both the degree of hyperpolarization of the membrane (which is directly related to the strength of the stimulating pulse) and its duration are important. As a measure of the minimum stimulation energy, we calculated the area between the transmembrane voltage and the zero line at threshold for anode break responses. The integration area was bounded on the time axis by the time of application of the stimulus and that of the action potential upstroke (Fig. 8, *inset*). This

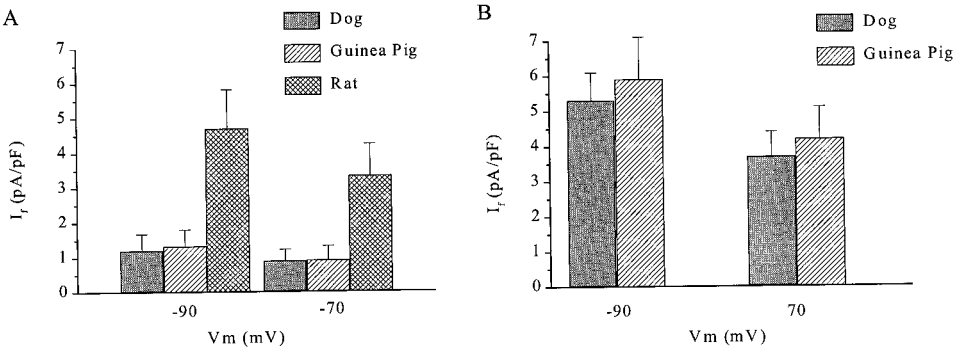

FIGURE 6 I_f tail currents in dog, guinea pig, and rat cells. (*A*) The myocytes were held at −150 mV for 2 s, and then the tail current was measured at a test potential of −70 and −90 mV ($n = 5$ for dog and rat, $n = 4$ for guinea pig). (*B*) The cell was held at −180 mV for 2 s, and the current was measured at test potentials of −70 and −90 mV.

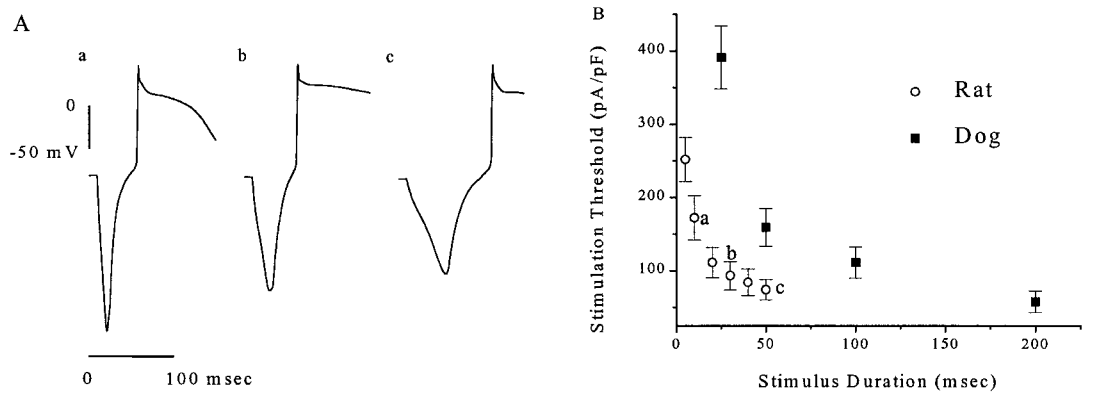

FIGURE 7 Strength-duration curve. (*A*) Representative action potentials recorded in rat myocytes for different stimulus pulse durations and strengths. (*B*) Stimulus strength-duration curve for dog and rat myocytes ($n = 5$).

measure of stimulation energy (in units of mV · ms) was compared with the amount of I_f activated in myocytes of different species after a hyperpolarizing pulse to −150 mV for 2 s. Fig. 8 shows that there is a strong correlation between the magnitude of I_f and the stimulus energy. A larger I_f is activated in rat than in guinea pig or dog cells, and thus cells from rats require less energy to achieve anode break stimulation. Interestingly, preliminary experiments using younger rats (6–10 weeks old) revealed that anode break responses were much more difficult to elicit than in the 6–22-month-old animals used here. This is consistent with the reported paucity of I_f in younger rats (Cerbai et al., 1996).

Action potential model

The action potential model developed by Luo and Rudy (1991) was implemented, and simulations were performed

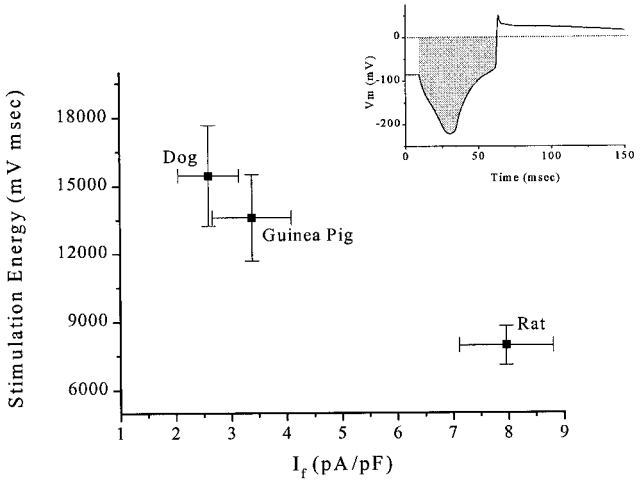

FIGURE 8 Stimulation energy versus I_f current magnitude. As a measure of stimulation energy needed for excitation at threshold, the transmembrane potential curve was integrated between the time of application of the stimulus pulse and the action potential upstroke (*inset*). The magnitude of I_f activated was determined by holding the cells at −150 mV for 2 s and measuring I_f at the end of the pulse. Rat myocytes have a larger I_f and require a lower stimulation energy for activation.

to test for anodal excitation. Fig. 9 shows the response of the unmodified model to cathodal (Fig. 9 *A*) and anodal (Fig. 9 *B*) stimulation. Anodal stimulation produces hyperpolarization of the cell, which returns monotonically to the resting potential upon the release of the pulse. The model was then modified to include I_f as well as the time-dependent blocking and unblocking of I_{K1}. The gating variables added to represent the time and voltage dependence of the currents were based on the experimental results presented above, using those from guinea pig whenever possible, given that the Luo-Rudy model is a guinea pig action potential model. The major differences among action potential models for different species are in the currents that underlie repolarization. Because we are concentrating on the mechanism of excitation, which relies primarily on the ubiquitous sodium current, the results are expected to be generalizable.

Fig. 9 (*C* and *D*) shows the results of simulations using the modified model. The response to cathodal stimulation shown in Fig. 9 *C* is the same as that of the unmodified model (Fig. 9 *A*). However, the response to anodal stimulation is qualitatively different: unlike the original model (Fig. 9 *B*), the modified model exhibits anode break stimulation (Fig. 9 *D*).

Fig. 10 shows the currents that are active during a stimulating pulse (shown here as a voltage clamp step for simplicity), and in the interval preceding the anode break action potential. Note the time-dependent reduction of I_{K1} (Fig. 10 *B*) and activation of I_f (Fig. 10 *C*) during the stimulus pulse. Upon the break of the pulse, I_f remains inward and drives the potential to more depolarized levels until the threshold for activation of the sodium current is reached and the upstroke occurs. Fig. 10 *D* shows the total current; the large inward peak represents the sodium current underlying the action potential upstroke.

We then determined whether the modified model could reproduce the experimentally observed stimulation-strength duration curve. Fig. 11 *A* shows the action potentials generated using the model for different stimulus durations at threshold, and Fig. 11 *B* is the simulated strength-duration curve. The absolute threshold of excitation differs from the

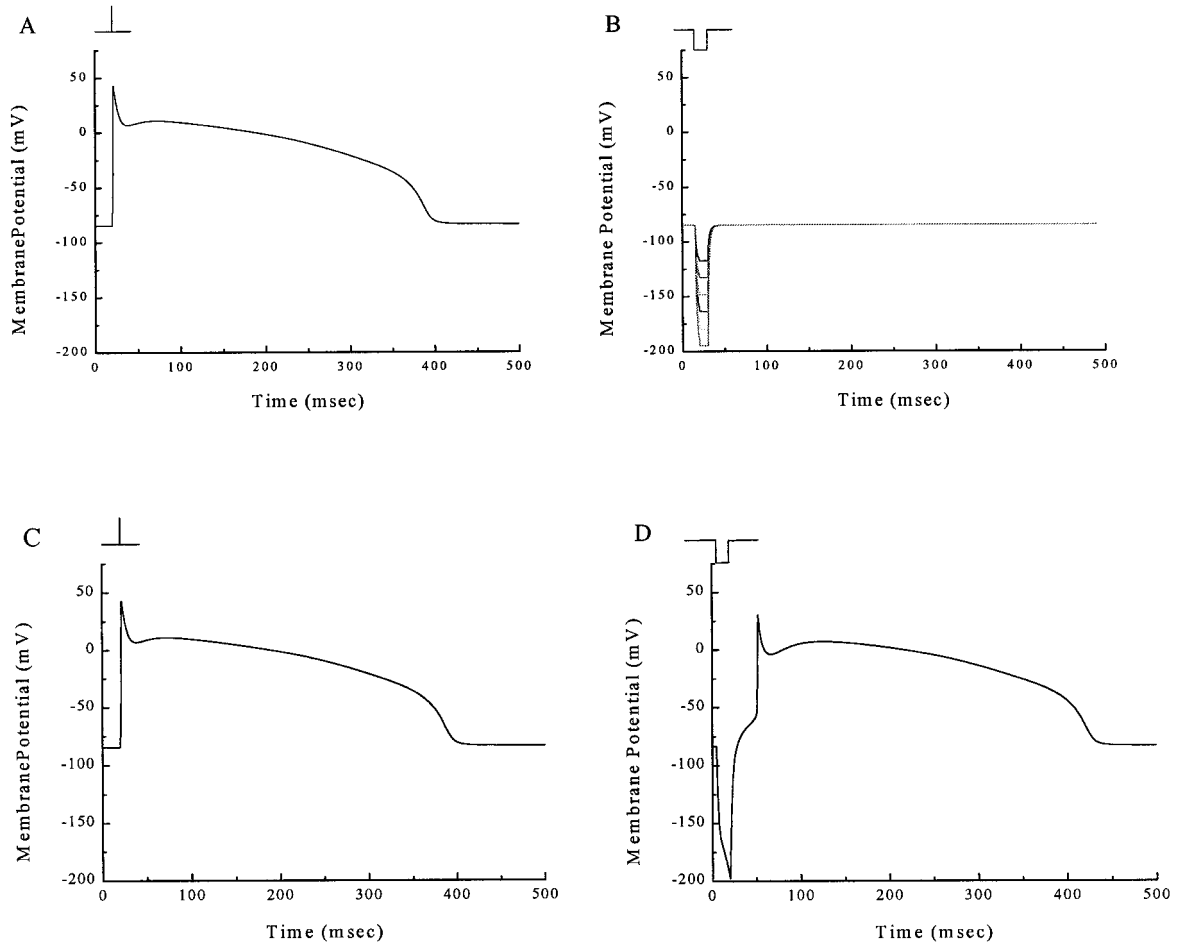

FIGURE 9 Action potential model. (*A* and *B*) Results of simulations using the unmodified Luo-Rudy model for cathodal and anodal stimulation, respectively. Anodal stimulation results in hyperpolarization of the cell, which returns to normal resting potential at the termination of the pulse. The bar at the top of the figures indicates the application of the stimulus pulse. For cathodal stimulation a 2-ms pulse was applied, and for anodal stimulation a 15-ms pulse was applied. (*C* and *D*) Result of simulations using the modified Luo-Rudy model for cathodal and anodal stimulation, respectively. The response of the modified model to cathodal stimulation is the same as that of the unmodified model. In response to anodal stimulation, the modified model exhibits anode break stimulation. The stimulus pulse durations are the same as in *A* and *B*.

experimentally determined values in Fig. 6, presumably because the model simulates the kinetics at 37°C, whereas the experiments were carried out room temperature. The current kinetics used in the model are considerably faster at 37°C for I_f because of the high Q_{10} of 3 (Hart, 1983). Nevertheless, the overall agreement with the results is remarkable (compare Figs. 6 and 11).

To gauge the relative importance of I_f and I_{K1} in the process of anode break stimulation, simulations were performed with action potential models that 1) included I_f but no I_{K1} block, 2) had no I_f but included I_{K1} block, and 3) included both I_f and I_{K1} block. Fig. 12 shows the results of current clamp simulations run for the same stimulus strength and duration for the three cases. In Fig. 12 *a*, with no I_{K1} block present in the model, anode break stimulation is not observed at this stimulus strength, even though the deactivating I_f does drive the transmembrane potential above the resting level (*inset*). The slight decrease in the magnitude of I_{K1} observed toward the end of the current clamp pulse is because of activation of inward I_f, which drives the membrane potential to more depolarized levels, reducing the driving force for I_{K1}. For higher stimulus strengths, anode break stimulation could be observed (not shown) when enough I_f was activated to drive the potential to the threshold for activation of the sodium current. In Fig. 12 *b*, with no I_f present in the model, no anode break stimulation could be generated. With the time-dependent reduction of I_{K1} conductance during the stimulus pulse, the cell is hyperpolarized to a greater extent than in Fig 12 *a*, even though the stimulus strength remains the same. Nevertheless, with no I_f present in the model, there is no net inward current to drive the transmembrane potential above the resting level, and hence no anode break stimulation can occur. This was the case even with very strong hyperpolarizations. In Fig. 12 *c*, with both I_f and I_{K1} block present, anode break stimulation is faithfully reproduced.

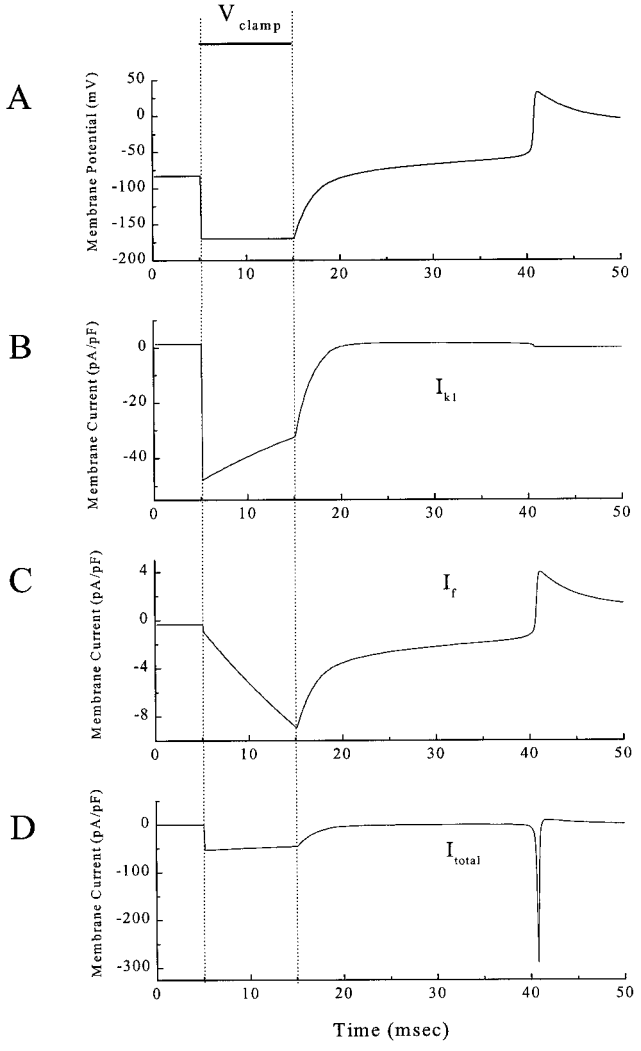

FIGURE 10 The role of different currents in the generation of anodal stimulation. The modified Luo-Rudy model was used for those simulations in which the cell was clamped at −170 mV for 10 ms (indicated by the *vertical dotted lines*). (*A*) The transmembrane potential. (*B*) The inward rectifier I_{K1} current. Note the reduction in current with time during the voltage clamp pulse. (*C*) Hyperpolarization-activated I_f current. The current is activated by the hyperpolarizing pulse and is inward until the action potential upstroke occurs, providing the current needed to drive the transmembrane potential to the threshold of activation for the sodium current. (*D*) Total current. The large inward current is the sodium current coinciding with the action potential upstroke.

Role of sodium channels in anode break stimulation

The classical explanation of anode break stimulation, as proposed by Hodgkin and Huxley (1952; see also Plonsey and Barr, 1988), involves a mechanism entirely different from that proposed here. In the squid, sodium channels were not fully reprimed at the resting potential. Hyperpolarization removed sodium current inactivation, and the larger sodium current upon release of the anodal pulse was postulated to bring the axon to threshold. In fact, our own implementation of the Hodgkin-Huxley equations reveals that repriming of sodium channels does not suffice; the details of the nonempirical leak current term are absolutely crucial for obtaining an anode break response (Ranjan, 1997). Nevertheless, we investigated the role of the sodium current in the cardiac action potential model. Fig. 13 *A* shows the simulated responses to anodal stimuli (*top*), the changes in sodium current activation (*m*) and inactivation (*h*) gating variables (*middle*), and the sodium current as a function of time for the various permutations of the model used in Fig. 12. The same stimulus strength and duration were used in all three cases. In the Luo-Rudy model, almost all of the sodium channels are available at rest, and thus there is no significant increase in the sodium current after the hyperpolarizing pulse. The sodium current plays a role only insofar as its recruitment underlies the action potential upstroke. One might argue that this is not a fair test of the Hodgkin-Huxley idea, because $h_\infty > 0.95$ at rest. We thus set $h_\infty = 0.7$ at the resting potential by shifting the h_∞ curve and reran the simulations. Fig. 13 *B* shows that such a change did not materially affect the conclusions. Even with a shifted h_∞ curve, there is no anode break response in the absence of I_f. In further simulations, we determined how the changes in h_∞ influenced the amount of current minimally required to induce an anode break response. Surprisingly, the model with a left-shifted h_∞ (as in Fig. 13 *B*) required more current injection to fire an action potential than did that in Fig. 13 *A* (56.8 pA/pF versus 56.1 pA/pF), consistent with the fact that it is harder to reach threshold with a left-shifted h_∞ curve. Similar reasoning rationalizes why the sodium current is smaller in Fig. 13 *B*(*c*) than in Fig. 13 *A*(*c*) (note the difference in *y* axis scales).

DISCUSSION

Anodal stimulation of the heart has been investigated for many years. Recently, anodal stimulation of cardiac tissue has been rationalized on the basis of passive cardiac tissue properties (Wikswo et al., 1995). In this study we investigated the role of active membrane properties during anodal stimulation. If active mechanisms suffice to produce anodal stimulation, isolated ventricular cells should manifest excitability in response to anodal stimulation. Isolated cell preparations eliminate the passive network tissue properties that have been postulated to underlie anodal excitation in multicellular preparations. Anodally induced action potentials were routinely recorded in isolated cells (Fig. 1), verifying that anodal stimulation can arise exclusively from active cardiac tissue properties. To stimulate any excitable tissue, a net inward current is required to drive the transmembrane potential to more depolarized levels. This net increase in the inward current could arise from an increase in inward current or a decrease in outward current flowing through the membrane, or a combination of both. We propose that both components are active in bringing about anode break stimulation.

A hyperpolarization-activated inward current has recently been recognized in mammalian ventricular cells (Yu et al.,

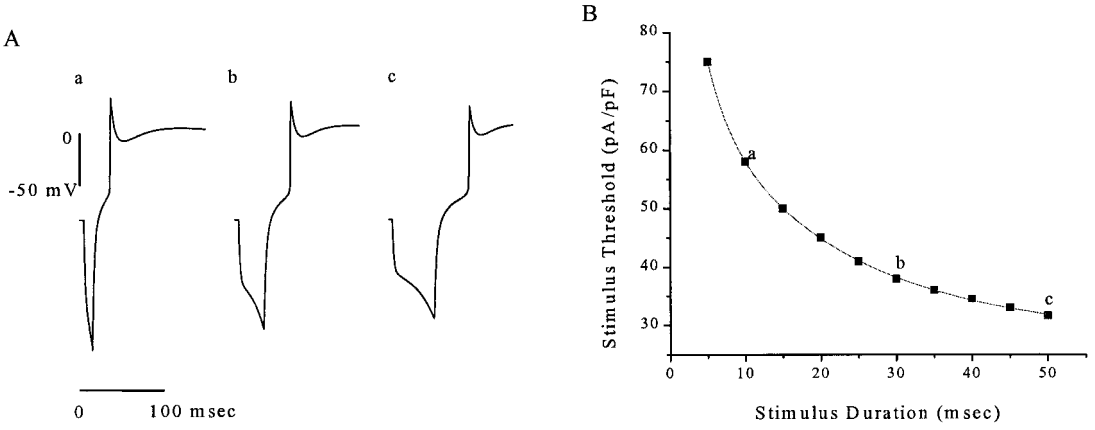

FIGURE 11 Strength-duration curve determined using the model. (*A*) The action potentials generated with the modified model at threshold for varying stimulus durations. (*B*) The stimulus strength-duration curve determined with the model.

1995; Cerbai et al., 1996). The presence of this current was verified in our canine, guinea pig, and rat ventricular cells (Fig. 4, *A–C*), and its biophysical characteristics were determined. In particular, we quantified the kinetics of deactivation at potentials relevant to anode break stimulation. This current is activated at voltages (Fig. 4 *D*) well within the range predicted in the tissue beneath a stimulating electrode during anodal stimulation (Roth, 1995). The current was also found to have rather slow activation and deactivation properties, similar to the pacemaker current I_f, which has been well characterized in cardiac nodal cells and in Purkinje fibers (Yanagihara and Irisawa, 1980; DiFrancesco et al., 1986; van Ginneken and Giles, 1991). This hyperpolarization-activated current was found to be carried by both sodium and potassium ions (Table 1), as previously reported (DiFrancesco, 1981; Yu et al., 1995). The reversal potential for this current is between that of sodium and potassium ions, making it an inward current at potentials near the action potential threshold. We propose that this inward current is indeed I_f and that it is recruited during anodal stimulation, thus providing the increase in inward current needed to drive the transmembrane potential to the threshold of the sodium current. Because the activation time constant for I_f is large, longer hyperpolarizing pulses were expected to lower the stimulation threshold. This prediction was experimentally verified, as shown in Fig. 6 and faithfully reproduced by the model (Fig. 11).

Fig. 10, which is based on simulations done using the modified Luo-Rudy model (after the inclusion of I_f and I_{K1} block/unblock), shows that the inward current needed to drive the transmembrane potential to threshold is provided by hyperpolarization-activated current. In the unmodified model, an anodal pulse results in hyperpolarization and time-independent activation of I_{K1} current. Because the transmembrane potential is below E_K at the termination of the stimulus pulse, I_{K1} provides the inward current needed to drive the potential toward the resting level. As there is no net inward current above E_K, the cell fails to depolarize any further and stays at the resting potential (Fig. 9 *B*), without eliciting an anode break response. Incorporation of I_f into the model provides the inward current needed to drive the membrane potential to threshold (Fig. 10 *D*), inducing the regenerative sodium current and hence the anode break stimulation.

Another current that is active at potentials below the resting membrane potential is the potassium current carried by inwardly rectifying I_{K1} channels. The ionic current carried by this channel is relatively large and is blocked at negative potentials in a time-dependent fashion by the cations present in normal physiological solutions. If the unblocking at the termination of the hyperpolarizing stimulus is time dependent as well, then the outward current carried by this channel above E_K will be reduced until the channel is fully unblocked. This reduction in the outward current component would potentiate the effect of any inward current in depolarizing the membrane. The time-dependent unblocking of I_{K1} was verified experimentally and quantified (Fig. 3). Simulations performed using the models with and without I_{K1} block (Fig. 12) demonstrate that the threshold for stimulation is higher when there is no I_{K1} block. Hence, even though the hyperpolarization-induced block of I_{K1} cannot lead to anode break stimulation on its own, it assists in the process by lowering the threshold for excitation.

Hodgkin and Huxley proposed a different explanation for anode break stimulation in squid axons (Hodgkin and Huxley, 1952). During hyperpolarization, inactivation of the sodium channel is removed (Plonsey and Barr, 1988); the enhanced sodium current upon release of the hyperpolarizing pulse results in an action potential. However, contemporary action potential models (Beeler and Reuter, 1977; Luo and Rudy, 1994), based on experimental results (Beeler and Reuter, 1970; Colatsky, 1980), assume very little steady-state inactivation of the sodium current at the resting potential (e.g., the Luo-Rudy model uses $h = 0.98$ at a resting transmembrane potential of -85 mV, where $h = 1.0$ represents no inactivation and $h = 0$ represents complete inactivation). Accordingly, the Luo-Rudy (1991) action potential model predicts that the cell will hyperpolarize during

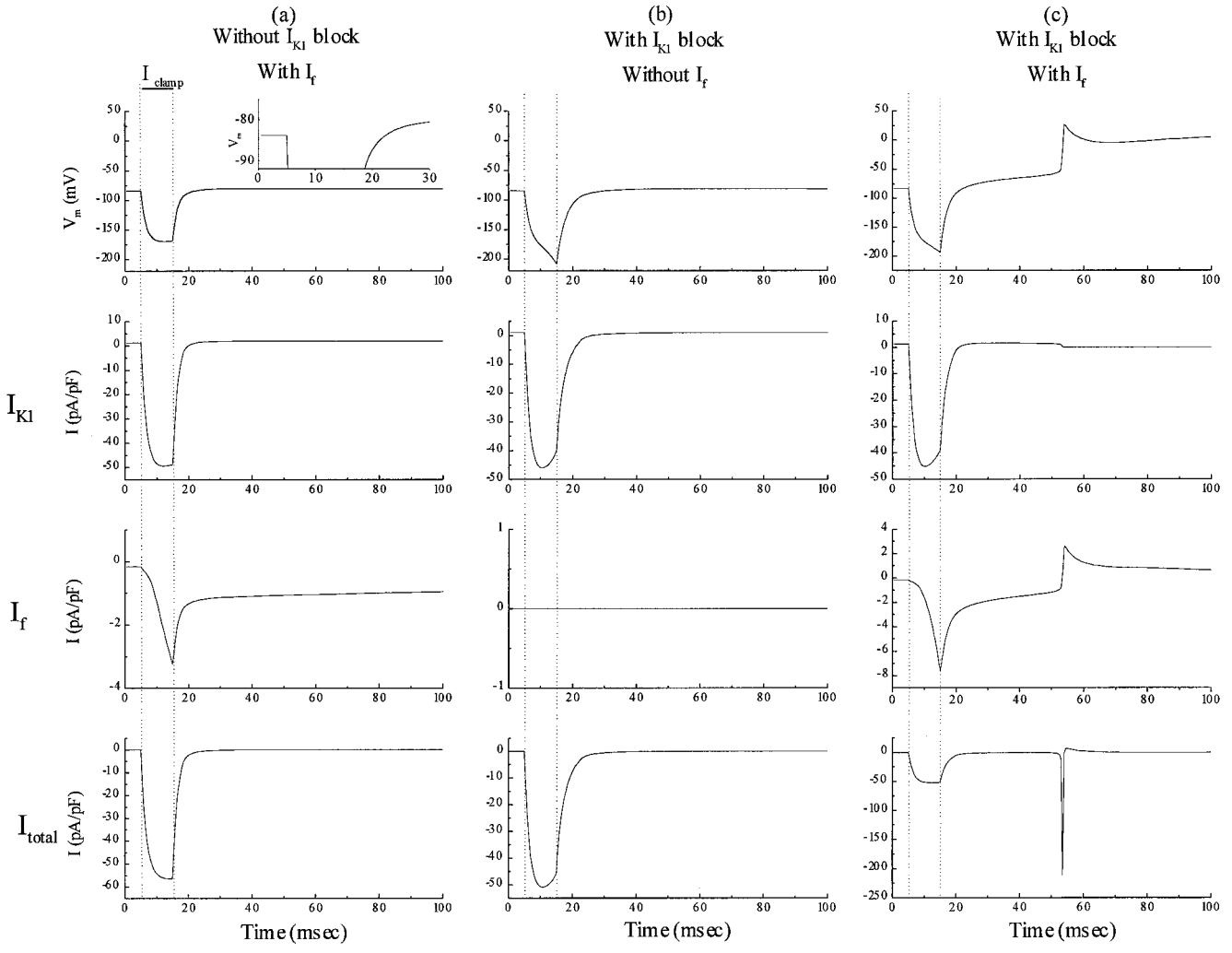

FIGURE 12 Result of simulations done with the models, with (*a*) time-independent I_{K1} and I_f; (*b*) time-dependent I_{K1} and no I_f; and (*c*) time-dependent I_{K1} and I_f. The results of model *a* are shown in the first column with the transmembrane potential in row 1, I_{K1} in row 2, I_f in row 3, and I_{total} in row 4. All of the current clamp simulations in this figure are of the same stimulus strength. Model *a* did not elicit an anode break response at this stimulus strength. I_f was activated during the pulse and provided the inward current to drive the membrane potential above the resting potential (shown in the *inset* on an expanded scale), but was not enough to elicit an action potential. Results of model *b* are shown in column 2. There is a reduction of I_{K1} current during the stimulus pulse, even though the driving force is increasing, simulating the block of the channel. Model *c* (column 3) exhibits an anode break response for this stimulus strength.

anodal stimulation and that the transmembrane potential will simply return monotonically to the resting level after cessation of the stimulus. It is possible that h_∞ is actually more hyperpolarized in heart cells than assumed by Luo-Rudy (Berman et al., 1989; Kimitsuki et al., 1990; Lawrence et al., 1991). Nevertheless, simulations done using the Luo-Rudy model with the h_∞ curve shifted such that $h = 0.7$ at rest did not result in an anode break response (Fig. 13 *B*). Moreover, the reported shift in h_∞ is largely based on cell-attached patch experiments and has been proposed to be due to increased membrane fluidity and surface potential effects of the glass pipette on the underlying membrane (Kimitsuki et al., 1990). Reports based on whole-cell preparations, using physiological internal ions, as in the present study, do not report any significant leftward shift of the h_∞ curve (Colatsky, 1980; Brown et al., 1981; Bodewei et al., 1982; Zilberter et al., 1982; Benndorf et al., 1985).

In conclusion, active membrane properties play a significant role in the process of anodal stimulation. The activation of I_f provides the current necessary to drive the potential to more depolarized levels, and the time-dependent block of I_{K1} aids the process by increasing membrane resistance. Thus, our findings provide a cellularly based rationale for anode break stimulation. Nevertheless, it must be emphasized that active membrane properties of the sort we have investigated do not help to rationalize anode make responses, i.e., stimulation that occurs during the hyperpolarization pulse itself. Bidomain theory remains the only viable explanation currently available for this phenomenon (Roth, 1995; Wikswo et al., 1995).

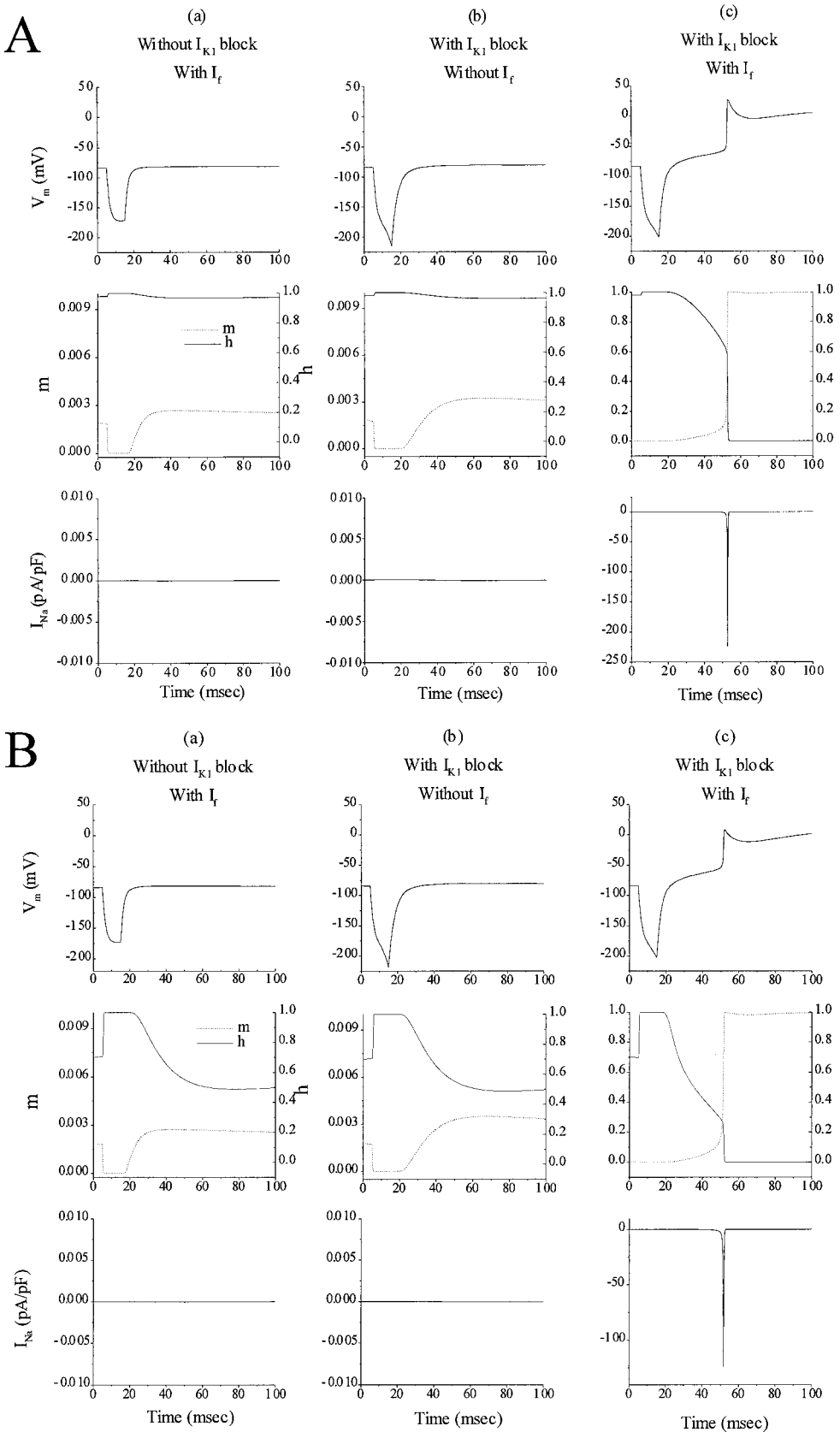

FIGURE 13 Results of simulations performed to test the role of sodium current in anode break excitation. In each panel, the top row shows the transmembrane potential, the middle row shows the value of activation (m) and inactivation (h) variables, and the bottom row shows the sodium current. All of the current clamp simulations in this figure are of the same stimulus strength, with a 10-ms pulse applied at time = 5 ms. For *A*, the kinetics for the sodium channel were the same as in the Luo-Rudy model. For *B* the sodium channel h_∞ curve was shifted such that only 70% of the channels are available at rest.

This study was supported by National Institutes of Health grant R37HL36957.

REFERENCES

Beeler, G. W., Jr., and H. Reuter. 1970. Voltage clamp experiments on ventricular myocardial fibres. *J. Physiol. (Lond).* 207:165–190.

Beeler, G. W., and H. Reuter. 1977. Reconstruction of the action potential of ventricular myocardial fibres. *J. Physiol. (Lond.).* 268:177–210.

Benndorf, K., W. Boldt, and B. Nilius. 1985. Sodium current in single myocardial mouse cells. *Pflugers Arch.* 404:190–196.

Berman, M. F., J. S. Camardo, R. B. Robinson, and S. A. Siegelbaum. 1989. Single sodium channels from canine ventricular myocytes: voltage dependence and relative rates of activation and inactivation. *J. Physiol. (Lond.).* 415:503–531.

Biermans, G., J. Vereecke, and E. Carmeliet. 1987. The mechanism of the inactivation of the inward-rectifying K current during hyperpolarizing steps in guinea-pig ventricular myocytes. *Pflugers Arch.* 410:604–613.

Biermans, G., J. Vereecke, and E. Carmeliet. 1989. Effect of external K on the block of the inward rectifier during hyperpolarization in guinea-pig ventricular myocytes by external Na. *Biomed. Biochim. Acta.* 48: S358–S363.

Bodewei, R., S. Hering, B. Lemke, L. V. Rosenshtraukh, A. I. Undrovinas, and A. Wollenberger. 1982. Characterization of the fast sodium current in isolated rat myocardial cells: simulation of the clamped membrane potential. *J. Physiol. (Lond).* 325:301–15.

Brooks, C. M., B. F. Hoffman, and E. E. Suckling 1955. Excitability of the Heart. Grune and Stratton, New York. 82–123.

Brown, A. M., K. S. Lee, and T. Powell. 1981. Sodium current in single rat heart muscle cells. *J. Physiol. (Lond).* 318:479–500.

Carmeliet, E. 1980. Decrease of K efflux and influx by external Cs ions in cardiac Purkinje and muscle cells. *Pflugers Arch.* 383:143–150.

Cerbai, E., M. Barbieri, and A. Mugelli. 1994. Characterization of the hyperpolarization-activated current, *I*(*f*), in ventricular myocytes isolated from hypertensive rats. *J. Physiol. (Lond.).* 481:585–591.

Cerbai, E., M. Barbieri, and A. Mugelli. 1996. Occurrence and properties of the hyperpolarization-activated current If in ventricular myocytes from normotensive and hypertensive rats during aging. *Circulation.* 94:1674–1681.

Cerbai, E., R. Pino, F. Porciatti, G. Sani, M. Toscano, M. Maccherini, G. Giunti, and A. Mugelli. 1997. Characterization of the hyperpolarization-activated current, If, in ventricular myocytes from human failing heart. *Circ.* 95:568–571.

Colatsky, T. J. 1980. Voltage clamp measurements of sodium channel properties in rabbit cardiac Purkinje fibres. *J. Physiol. (Lond.).* 305: 215–234.

Cranefield, P. F., B. F. Hoffman, and A. A. Siebens. 1957. Anodal excitation of cardiac muscle. *Am. J. Physiol.* 190:383–390.

Dekker, E. 1970. Direct current make and break thresholds for pacemaker electrodes on the canine ventricle. *Circ. Res.* 27:811–823.

DiFrancesco, D. 1981. A study of the ionic nature of the pace-maker current in calf Purkinje fibres. *J. Physiol. (Lond.).* 314:377–393.

DiFrancesco, D., A. Ferroni, M. Mazzanti, and C. Tromba. 1986. Properties of the hyperpolarizing-activated current (if) in cells isolated from the rabbit sino-atrial node. *J. Physiol. (Lond.).* 377:61–88.

DiFrancesco, D., and D. Noble. 1985. A model of cardiac electrical activity incorporating ionic pumps and concentration changes. *Philos. Trans. R Soc. Lond. Biol.* 307:353–398.

Furman, S., D. L. Hayes, and D. R. Holmes 1989. A Practice of Cardiac Pacing. Futura Publishing Co., Mount Kisco, NY. 39–42.

Hamill, O. P., A. Marty, E. Neher, B. Sakmann, and F. J. Sigworth. 1981. Improved patch-clamp techniques for high-resolution current recording from cells and cell-free membrane patches. *Pflugers Arch.* 391:85–100.

Hart, G. 1983. The kinetics and temperature dependence of the pace-maker current If in sheep Purkinje fibres. *J. Physiol. (Lond.).* 337:401–416.

Henriquez, C. S. 1993. Simulating the electrical behavior of cardiac tissue using the bidomain model. *Crit. Rev. Biomed. Eng.* 21:1–77.

Henriquez, C. S., N. Trayanova, and R. Plonsey. 1990. A planar slab bidomain model for cardiac tissue. *Ann. Biomed Eng.* 18:367–376.

Hodgkin, A. L., and A. F. Huxley. 1952. A quantitative description of membrane current and its application to conduction and excitation in nerve. *J. Physiol. (Lond.).* 117:500–544.

Hoffman, B. F., and P. F. Cranefield 1960. Electrophysiology of the Heart. McGraw-Hill, New York. 211–233.

Kääb, S., H. B. Nuss, N. Chiamvimonvat, B. O. Rourke, P. H. Pak, D. A. Kass, E. Marban, and G. F. Tomaselli. 1996. Ionic mechanism of action potential prolongation in ventricular myocytes from dogs with pacing-induced heart failure. *Circ Res.* 78:262–273.

Kimitsuki, T., T. Mitsuiye, and A. Noma. 1990. Negative shift of cardiac Na^+ channel kinetics in cell-attached patch recordings. *Am. J. Physiol.* 258:H247–H54.

Lawrence, J. H., D. T. Yue, W. C. Rose, and E. Marban. 1991. Sodium channel inactivation from resting states in guinea-pig ventricular myocytes. *J. Physiol. (Lond.).* 443:629–650.

Liu, Y., W. D. Gao, B. O. Rourke, and E. Marban. 1996. Synergistic modulation of ATP-sensitive K^+ currents by protein kinase C and adenosine. Implications for ischemic preconditioning. *Circ Res.* 78: 443–454.

Luo, C. H., and Y. Rudy. 1991. A model of the ventricular cardiac action potential. Depolarization, repolarization, and their interaction. *Circ Res.* 68:1501–1526.

Luo, C. H., and Y. Rudy. 1994. A dynamic model of the cardiac ventricular action potential. I. Simulations of ionic currents and concentration changes. *Circ Res.* 74:1071–1096.

Mitra, R. L., and M. Morad. 1991. Permeance of Cs^+ and Rb^+ through the inwardly rectifying K^+ channel in guinea pig ventricular myocytes. *J. Membr. Biol.* 122:33–42.

Plonsey, R., and R. C. Barr. 1984. Current flow patterns in two-dimensional anisotropic bisyncytia with normal and extreme conductivities. *Biophys. J.* 45:557–571.

Plonsey, R., and R. C. Barr. 1988. Bioelectricity: A Quantitative Approach. Plenum Press, New York. 85–96.

Pollard, A. E., N. Hooke, and C. S. Henriquez. 1992. Cardiac propagation simulation. *Crit. Rev. Biomed. Eng.* 20:171–210.

Press, W. H., S. A. Teukolasky, W. T. Vetterling, and B. P. Flannery 1992. Numerical Recipes in FORTRAN. Cambridge University Press, New York. 701–744.

Ranjan, R. 1997. Mechanism of anodal stimulation in cardiac tissue. Ph.D. dissertation. The Johns Hopkins University, Baltimore, MD.

Ranjan, R., N. Chiamvimonvat, G. F. Tomaselli, and E. Marban. 1997. Mechanism of anodal stimulation in cardiac ventricular myocyte. *Biophys. J.* 72:A110 (Abstr.).

Roth, B. J. 1988. The electrical potential produced by a strand of cardiac muscle: a bidomain analysis. *Ann. Biomed. Eng.* 16:609–637.

Roth, B. J. 1992. How the anisotropy of the intracellular and extracellular conductivities influences stimulation of cardiac muscle. *J. Math Biol.* 30:633–646.

Roth, B. J. 1994. Mechanisms for electrical stimulation of excitable tissue. *Crit. Rev. Biomed. Eng.* 22:253–305.

Roth, B. J. 1995. A mathematical model of make and break electrical stimulation of cardiac tissue by a unipolar anode or cathode. *IEEE Trans. Biomed. Eng.* 42:1174–1184.

Roth, B. J. 1996. Strength-interval curves for cardiac tissue predicted using the bidomain model. *J. Cardiovasc. Electrophysiol.* 77:722–737.

Roth, B. J., and J. P. Wikswo, Jr. 1994. Electrical stimulation of cardiac tissue: a bidomain model with active membrane properties. *IEEE Trans. Biomed. Eng.* 41:232–240.

Sepulveda, N. G., B. J. Roth, and J. P. Wikswo, Jr. 1989. Current injection into a two-dimensional anisotropic bidomain. *Biophys. J.* 55:987–999.

Sepulveda, N. G., and J. P. Wikswo, Jr. 1994. Bipolar stimulation of cardiac tissue using an anisotropic bidomain model. *J. Cardiovasc. Electrophysiol.* 5:258–267.

van Ginneken, A. C., and W. Giles. 1991. Voltage clamp measurements of the hyperpolarization-activated inward current *I*(*f*) in single cells from rabbit sino-atrial node. *J. Physiol. (Lond.).* 434:57–83.

Wikswo, J. P., Jr. 1994. The complexities of cardiac cables: virtual electrode effects. *Biophys. J.* 66:551–553.

Wikswo, J. P., Jr., S. F. Lin, and R. A. Abbas. 1995. Virtual electrodes in cardiac tissue: a common mechanism for anodal and cathodal stimulation. *Biophys. J.* 69:2195–2210.

Yanagihara, K., and H. Irisawa. 1980. Inward current activated during hyperpolarization in the rabbit sinoatrial node cell. *Pflugers Arch.* 385:11–19.

Yu, H., F. Chang, and I. S. Cohen. 1993. Pacemaker current exists in ventricular myocytes. *Circ Res.* 72:232–236.

Yu, H., F. Chang, and I. S. Cohen. 1995. Pacemaker current $i(f)$ in adult canine cardiac ventricular myocytes. *J. Physiol. (Lond.).* 485:469–483.

Zilberter, Y. I., E. N. Timin, Z. A. Bendukidze, and N. A. Burnashev. 1982. Patch-voltage-clamp method for measuring fast inward current in single rat heart muscle cells. *Pflugers Arch.* 394:150–155.